



NRVS and DFT of MitoNEET: Understanding the Special Vibrational Structure of a [2Fe-2S] Cluster with (Cys)₃(His)₁ Ligation

Leland Gee, Vladimir Pelmeshnikov, Cécile Mons, Nakul Mishra, Hongxin Wang, Yoshitaka Yoda, Kenji Tamasaku, Marie-Pierre Golinelli-Cohen, Stephen Cramer

► To cite this version:

Leland Gee, Vladimir Pelmeshnikov, Cécile Mons, Nakul Mishra, Hongxin Wang, et al.. NRVS and DFT of MitoNEET: Understanding the Special Vibrational Structure of a [2Fe-2S] Cluster with (Cys)₃(His)₁ Ligation. *Biochemistry*, 2021, 60 (31), pp.2419-2424. <10.1021/acs.biochem.1c00252>. <hal-03312155>

HAL Id: hal-03312155

<https://hal.science/hal-03312155v1>

Submitted on 7 Oct 2021

HAL is a multi-disciplinary open access archive for the deposit and dissemination of scientific research documents, whether they are published or not. The documents may come from teaching and research institutions in France or abroad, or from public or private research centers.

L'archive ouverte pluridisciplinaire **HAL**, est destinée au dépôt et à la diffusion de documents scientifiques de niveau recherche, publiés ou non, émanant des établissements d'enseignement et de recherche français ou étrangers, des laboratoires publics ou privés.



HAL Authorization

NRVS and DFT of MitoNEET – Understanding the Special Vibrational Structure of a [2Fe-2S] Cluster with (Cys)₃(His)₁ Ligation

Leland B. Gee,[†] Vladimir Pelmeshnikov,[€] Cécile Mons,[‡] Nakul Mishra,[#] Hongxin Wang,^{\$}

Yoshitaka Yoda,[¥] Kenji Tamasaku,^{¥,§} Marie-Pierre Golinelli-Cohen,[‡] and Stephen P.

Cramer^{*,§}

[†] LCLS, SLAC National Accelerator Laboratory, Menlo Park, California 94025, USA

[€] Institut für Chemie, Technische Universität Berlin, 10623 Berlin, Germany

[#] Department of Chemistry, University of California, Davis, California 95616, USA

[¥] Precision Spectroscopy Division, SPring-8/JASRI, 1-1-1 Kouto, Sayo, Hyogo 679-5198, Japan

[§] RIKEN SPring-8 Center, 1-1-1 Kouto, Sayo-cho, Sayo-gun, Hyogo 679-5148, Japan

[‡] Institut de Chimie des Substances Naturelles (ICSN), CNRS UPR 2301, Université Paris-Saclay, 91198 Gif-sur-Yvette cedex, France

^{\$} SETI Institute, Mountain View, California 94043, USA

RECEIVED DATE ()

Running title: NRVS and DFT of mitoNEET

Abstract

The human mitochondrial protein, mitoNEET (mNT), belongs to the family of small [2Fe-2S] NEET proteins that bind their iron-sulfur clusters with a novel and characteristic 3Cys:1His coordination motif. mNT has been implicated in the regulation of lipid and glucose metabolisms, iron/reactive oxygen species homeostasis, cancer and possibly Parkinson's disease. The geometric structure of mNT as a function of redox state and pH is critical for its function. In this study we combine ⁵⁷Fe nuclear resonance vibrational spectroscopy (NRVS) with density functional theory (DFT) calculations to understand the novel properties of this important protein.

Keywords: mitoNEET, Fe-S cluster, NRVS, synchrotron radiation, vibrational spectroscopy, DFT

* Corresponding author: scramer@seti.org

Introduction

The NEET proteins comprise a family of small proteins that bind their iron-sulfur [2Fe-2S] clusters with a novel and characteristic 3Cys:1His coordination motif.¹ The human mitochondrial outer-membrane version, mitoNEET (mNT), was discovered as a potential target of insulin-sensitizing thiazolidinedione drugs.² It has since been found involved in the regulation of lipid and glucose metabolisms,³⁻⁴ iron/reactive oxygen species homeostasis⁴⁻⁶ with implication in cancer,⁷⁻⁹ and possibly Parkinson's disease.¹⁰ *In vitro* studies revealed that mNT can transfer its cluster to a recipient apoprotein¹¹ under the strict control of the redox state (only the oxidized cluster can be transferred)¹² and the regulation by pH level.¹² Using complementary *in cellulo* experiments, we demonstrated that mitoNEET is involved in the pathway dedicated to reactivation of cytosolic aconitase after an oxidative/nitrosative stress. *In vitro*, mitoNEET is able to transfer its clusters to the apoform of the cytosolic aconitase (IRP-1) and to reactive it.⁵

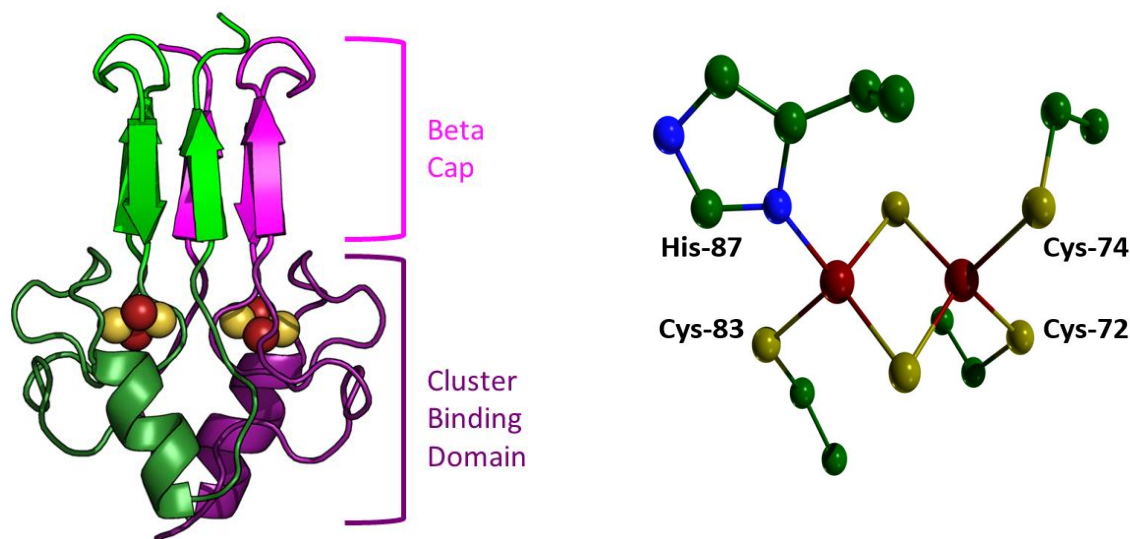


Figure 1. Left: the protein fold for mNT. Right: close-up of the 3Cys:1His [2Fe-2S] cluster up to the C α carbon of each residue with hydrogens omitted. The structures shown are based on PDB 2QH7.¹³

Crystal structures¹³⁻¹⁵ of mNT reveal a homodimeric fold with one [2Fe-2S] cluster per monomer and two domains: the cluster-binding domain and a beta cap, as shown in **Figure 1**.¹³ The presence of a histidine ligand to one Fe site confers some unusual properties to this cluster, including a pH-dependent redox potential higher than that of conventional [2Fe-2S]

ferredoxin (Fd) proteins,¹⁶ capability for proton-coupled electron transfer (PCET),¹⁷⁻¹⁸ and redox control¹⁹ and pH modulation¹² of its cluster-transfer activity.

The mNT protein has already been studied by a variety of spectroscopies, including UV-visible,^{5, 20} EPR,²⁰⁻²² NMR,^{5, 19} Mössbauer,^{5, 20} and Raman^{12, 23} techniques, as well as molecular dynamics.²⁴⁻²⁵ However, questions remain about the drastic difference of behaviors concerning cluster stability and transfer between the reduced and the oxidized forms of the protein. Of special importance, is the characterization of the Fe-His interaction through the coordinating N_δ atom. It has been proposed that this bond may play a role in the cluster lability.^{21, 23}

To better understand the special properties of the mNT [2Fe-2S] cluster and to gain insights into the role of the coordinating histidine for cluster lability, we have utilized nuclear resonance vibrational spectroscopy (NRVS) combined with density functional theory (DFT) calculations.

Results and Discussion

NRVS at pH 6.7. In our previous studies,¹² we demonstrated that the stability of the oxidized form of mNT decreases when the pH is more acidic. From pH 7.2 to 8, the oxidized form is quite stable, however the cluster stability significantly drops below pH 7. We decided to explore the oxidized and reduced form of mNT at pH 6.7 using NRVS, because this pH represents a good balance between cluster stability and physiological relevance.¹² The NRVS data for oxidized and reduced mNT are presented in **Figure 2a**. As previously observed with [2Fe-2S] **Fds**, the low frequency bands in the 50-120 cm⁻¹ range correspond to large scale protein motions and torsional modes of the [2Fe-2S] cluster, while the features from ~120 to 180 cm⁻¹ involve significant bending motion.²⁶ At the other extreme, modes around ~400 cm⁻¹ involve stretching of the Fe centers together with bridging sulfides (S_b). Upon reduction the bands are generally red-shifted by 10-20 cm⁻¹, although there is not an exact 1:1 correspondence in modes consistent with other Fe-S clusters.²⁷ For the oxidized spectrum, there is fair correspondence with the previously reported Raman spectrum (**Table S1**).²³

Qualitative assignment of the major features for the oxidized sample can be done by comparison with previous NRVS and Raman results on [2Fe-2S] Fds (**Table S1**). The pair of

high frequency bands (413 and 395 cm^{-1}) align with similar bands in *Rc6 Fd*.²⁶ From previous literature, these have been assigned respectively to asymmetric and symmetric motions of the [2Fe-2S] core.^{26, 28} The middle frequency bands ($\sim 300\text{-}373 \text{ cm}^{-1}$) correspond mostly to various mixtures of Fe-St(Cys) and Fe-S_b stretching motions.²⁸ The 295 cm^{-1} feature is not seen in the *Rc6 Fd* spectrum, but bands at 284 and 293 cm^{-1} are seen in the Raman spectrum of mNT; they are presumably Fe-St(Cys) stretches “influenced by the presence of the Fe-His moiety”.²³

The NRVS band at 260 cm^{-1} has no correspondences in conventional Fd spectra, but it can be related to bands seen at 267 and 265-274 cm^{-1} respectively in mNT²³ and Rieske protein²⁹ Raman spectra. In the latter case, bands at 266 and 274 cm^{-1} were assigned respectively to protonated-hydrogen-bonded imidazole and deprotonated-hydrogen-bonded imidazolate, both ligated to Fe with water serving as the H-bond donor/acceptor.³⁰

The reduced mNT NRVS shows the expected shifts to lower frequencies that were seen in Fd proteins (**Figure 2a**).²⁶ The primary Fe-S_b modes shift by 13 and 21 cm^{-1} to respectively 400 and 375 cm^{-1} , about the same as seen in Fds. Similar shifts are also seen in the Fe-St(Cys) region. The most dramatic shift is the presumed Fe-N₈(His) band migration from 260 down to 225 and 212 cm^{-1} . Since it is the His-ligated Fe that is redox active,²¹ the latter bands can be ascribed to the Fe(II)-N₈(His) motion.

Observation of this candidate Fe(II)-N₈(His) mode illustrates an advantage of the NRVS technique – the reduced species exhibits contributions to the NRVS signal of similar quality from both the Fe(II) and Fe(III) sites. In contrast, although resonance Raman spectra of reduced Rieske proteins have been reported,²⁹⁻³⁰ in both cases the authors concluded that the spectrum primarily reports on the Fe(III) site of this mixed valence species, because this is the source of the resonantly excited S \rightarrow Fe charge-transfer band. NRVS allows inspection of the mNT Fe(II)-N_{his} vibrational modes for the first time.

Analogies can be made to the resonance Raman spectra of deoxy-myoglobin (Mb), which also contains a high-spin Fe(II)-histidine bond. Bands at 210, 218, and 225 cm^{-1} have been reported for deoxy-Mb at 150K (or 213, 220, and 226 cm^{-1})³¹ and assigned to different conformational substates with respect to the Fe-His bond.³² It is unclear if the pair of features

at 212 and 225 cm^{-1} in the reduced mNT spectrum might analogously represent different conformations; for more detailed insights into these features, we turned to DFT calculations.

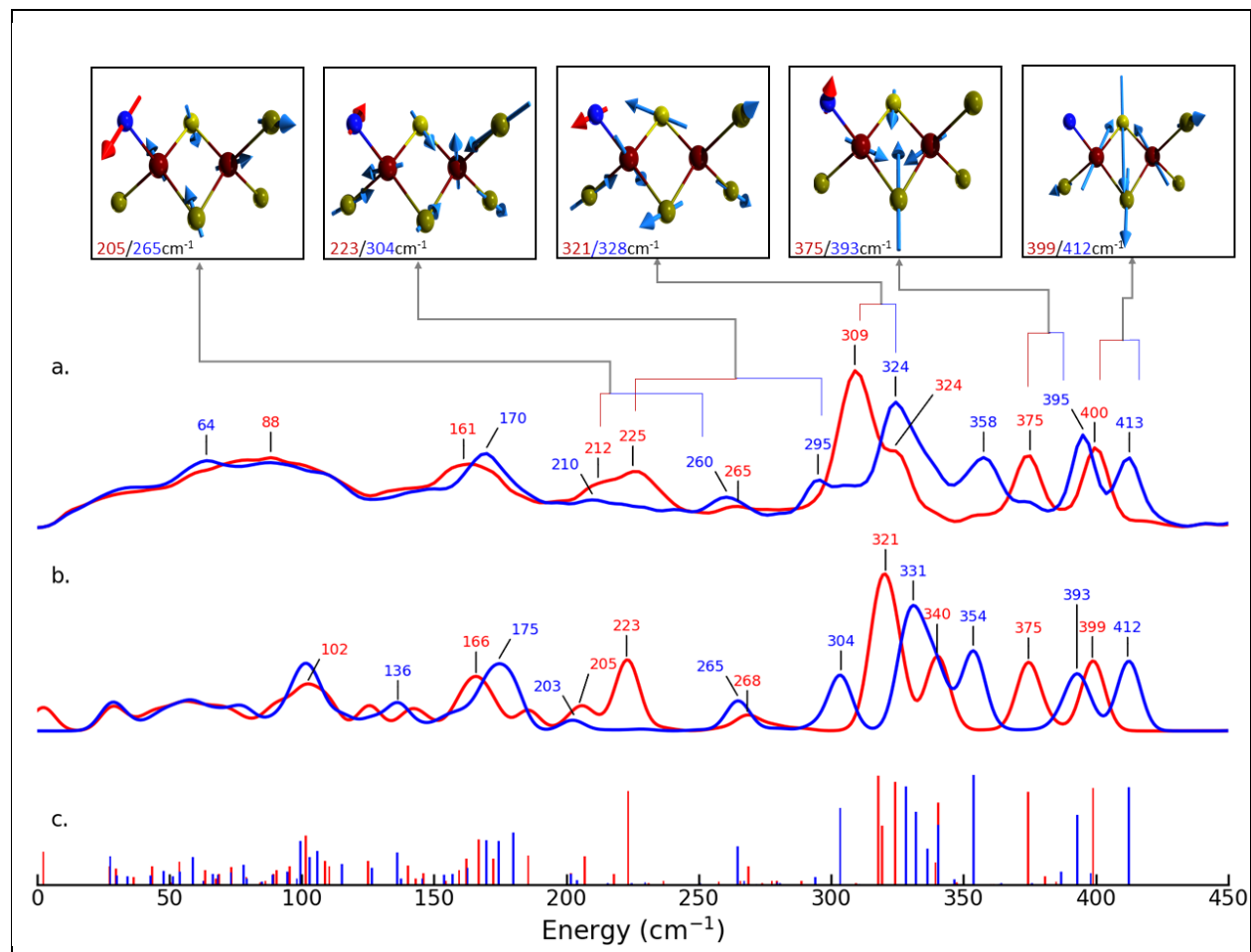


Figure 2. PVDOS for oxidized (—) and reduced (—) mNT: **a.** Experimental ^{57}Fe PVDOS (NRVS) spectrum; **b.** DFT calculated ^{57}Fe PVDOS spectrum; **c.** individual ^{57}Fe PVDOS calculated transitions. Upper inset shows DFT-calculated vibrational motion (arrows) and frequencies for the $[\text{2Fe-2S}]$ core with lines indicating their experimental assignment in the oxidized and reduced forms – motion depicted is of the $[\text{2Fe-2S}]^{2+}$ oxidized state calculation. Labels in the DFT-derived spectrum reflect band positions for comparison to experiment; the individual mode energies are available in **Table S1**.

We performed DFT calculations on a truncated model of mNT, involving the $[\text{2Fe-2S}]$ cluster and its immediate protein environment (**Figure S1**). The model includes the amino acid backbone linking the four residues directly coordinating the $[\text{2Fe-2S}]$ core, with the non-coordinating residues truncated to their C_α positions. The $[\text{2Fe-2S}]^{2+}$ and $[\text{2Fe-2S}]^{1+}$ states were calculated with and without protonation of the Fe-coordinating histidine (His-87). Regardless of the $\text{N}_\epsilon(\text{His-87})$ protonation status, our calculations indicated the histidine bound iron to be the redox-active metal site – which is reminiscent of reduced Rieske clusters

where the two histidine-bound Fe is reduced (see **Supporting Information** for details and alternative DFT models).³³ The best agreement with our experimental data is achieved by models with a coordinating histidine imidazole for the reduced form and an imidazolate for the oxidized forms, as shown by the simulated NRVS profiles in **Figure 2b**. The protonation of the histidine upon reduction at this pH = 6.7 level is consistent with previous pulsed EPR studies.²¹

For the oxidized cluster, starting from high energy, the 413/395 cm⁻¹ bands are confirmed to be asymmetric/symmetric Fe-S modes of the entire [2Fe-2S]²⁺ core respectively (**Supporting Information – animated vibrational modes**). The experimental pair of bands at 358/324 cm⁻¹ are dominantly Fe-S_t/N_δ(His) asymmetric stretching modes with the former mode strongly coupled to Fe-S_b motion and the latter representing the most intense feature in the spectrum. The intensity at 295 cm⁻¹ is of special note, inspection of this mode reveals a substantial Fe(III)-N_δ(His) stretching character weakly coupled to Fe-S_b scissoring motion and Fe-S_t stretching motion. Likewise, another experimental mode at 260 cm⁻¹ similarly features Fe-His stretching – but with much less coupling to Fe-S_t motion than the feature at 295 cm⁻¹ resulting in a lower ⁵⁷Fe PVDOS. A distribution of Fe-N_δ stretching-related modes in this region is consistent with previous resonance Raman data.²³

The experimental intensity observed at 170 cm⁻¹ in the oxidized cluster is predicted to be composed of multiple vibrational modes. These modes are essentially Fe-S_t/N_δ bending modes with the Fe atoms wagging relative to the coordinating amino acids. Below 100 cm⁻¹, broad intensity is observed that is composed of strongly delocalized vibrations coupled to the protein backbone; such modes are not predicted by the truncated models used by DFT, however we do note that our simulations predict another bending mode (calculated at 102 cm⁻¹) with the Fe and coordinating amino acids moving in a twisting motion that is contributing significant intensity in this region.

Upon reduction and protonation of the coordinating imidazole, our calculations verify a shift of the high energy (>300 cm⁻¹) Fe-S cluster modes to lower energy, with their characters otherwise similar to the oxidized state modes. The mode at 295 cm⁻¹ in the oxidized cluster is not present in the reduced system – implying a change in the Fe-N_δ bonding. There are two modes in the reduced spectrum calculated at 223 (**Figure 3**) and 207 cm⁻¹, which upon inspection respectively reflect the features at 295 and 260 cm⁻¹ calculated for the oxidized

cluster. Although the core [2Fe-2S] motion is similar, the reduced version of the modes features increased motion of both the directly cluster-coordinating and intervening amino acids (**Figure S1**). Finally, the low-energy region for the reduced cluster is again composed of various Fe-N_δ, Fe-S_t, and Fe-S_b bending modes with the strongest contribution from the Fe-S_t/N_δ wagging motion.

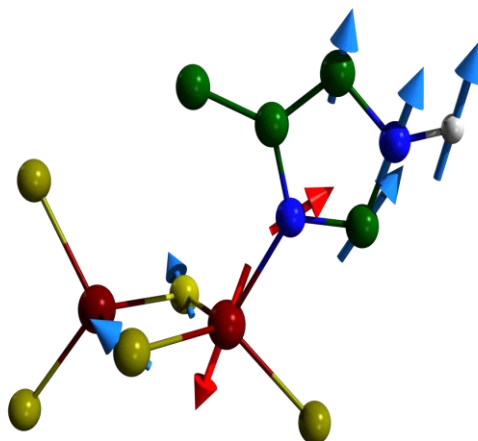


Figure 3. The reduced [2Fe-2S]¹⁺ state mNT mode calculated at 223 cm⁻¹, showing the Fe(II)-N_δ(His) stretch. Only the [2Fe-2S] and His-87 fragments of the DFT model are shown.

The decrease in frequency of the Fe-N_δ derived vibrations is consistent with our geometry optimized structure for the reduced cluster which predicts a 0.12 Å increase in the Fe-N_δ(His) bond upon cluster reduction and concomitant protonation of His-87 (**Supporting Information – DFT structures**). This is consistent with the greater donor character of imidazolate compared to imidazole.

Discussion

Previous work on holo-mNT in the oxidized and reduced states revealed very little modification of the tertiary and quaternary structure between the two forms.¹⁹ This fact is consistent with the minimal redox-dependent changes in the low energy region of the NRVS spectra that reflect diffuse vibrations strongly coupled to the protein backbone. The holo-mNT has been shown to be susceptible to cluster loss under oxidizing conditions⁵ and it has been proposed previously that Fe-N_δ(His) bond scission at low pH could operate as a first

step of cluster loss.²³ Our results verify that the Fe-His bond is stronger in the oxidized state relative to the reduced state, and at first glance the increased lability of the oxidized [2Fe-2S] mNT cluster (relatively to its reduced form) seems paradoxical.

Previously, it has been observed in deoxyMb that iron-histidine bond cleavage is driven by solvation and unfolding of the active site at lower pH rather than protonation of the Fe-coordinating imidazole.³⁴ One possible opportunity for the loss of the mNT cluster is the compression of the cluster upon oxidation. The nearby Lys-55 (from the other monomer), near the [2Fe-2S]-coordinating His-87, has been purported to dynamically hydrogen bond to the imidazolate and protect it from solvent exposure.²⁵ Our geometry optimized structures, that reflect our experimental NRVS data, demonstrate a shortening of the Fe-N_δ bond and of the opposing Fe-S_t bonds on the opposite side of the cluster (**Figure 4 - Right**).

We found including protonation of the N_ε to imidazole in the oxidized form into our DFT calculation leads to a relative increase 0.06 Å of the Fe-N_δ bond still 0.06 Å shorter than the reduced cluster. This lengthening reflects an increased labilization of the bond and possibly contributes to the pH dependence of the cluster loss. Likewise, protonation to imidazole would eliminate the direct N_ε to Lys-55 H-bonding.²⁵

Collectively, this implies that when the reduced cluster is oxidized under non-acidic conditions to [2Fe-2S]²⁺ there is a compression of the cluster geometry and coordinating histidine. Although not dramatically different, this new geometry reduces the dynamic residence time of the hydrogen bond between His-87 and Lys-55 (**Figure 4 - Left**) allowing greater solvent access into the protein cleft between the two amino acids (relative to the reduced form). Greater solvent access gives an enthalpic pressure for the Fe-N_δ bond rupture.²⁵ Further, at lower pH, the cluster-bound imidazole cannot interact with Lys-55 and the cleft can be dynamically solvated more frequently²⁵ – this is concomitant with increased destabilization of the Fe-N_δ bond due to the reduced donor character of imidazole vs. imidazolate to the Fe atom which would lead to enhanced geminate release of the [2Fe-2S]²⁺ cluster. This mechanism explains the redox-dependent cluster-loss and how it is enabled by lower pH in mitoNEET – but will require additional structural studies for confirmation. However, the model is consistent with many existing mutagenesis studies of the critical Lys-55. Substitution by a guanidinium in K55R²⁴ showed similar cluster stability to wildtype expected of a similar H-bonding pattern; conversion to the aliphatic residue K55I³⁵ observed

higher cluster stability than wildtype which is consistent with a reduced polarity of the protein cleft gated by K55 and H87 (**Figure 4 Left**); and conversion to an anionic residue in K55E¹¹ revealed slower cluster transfer than wildtype.

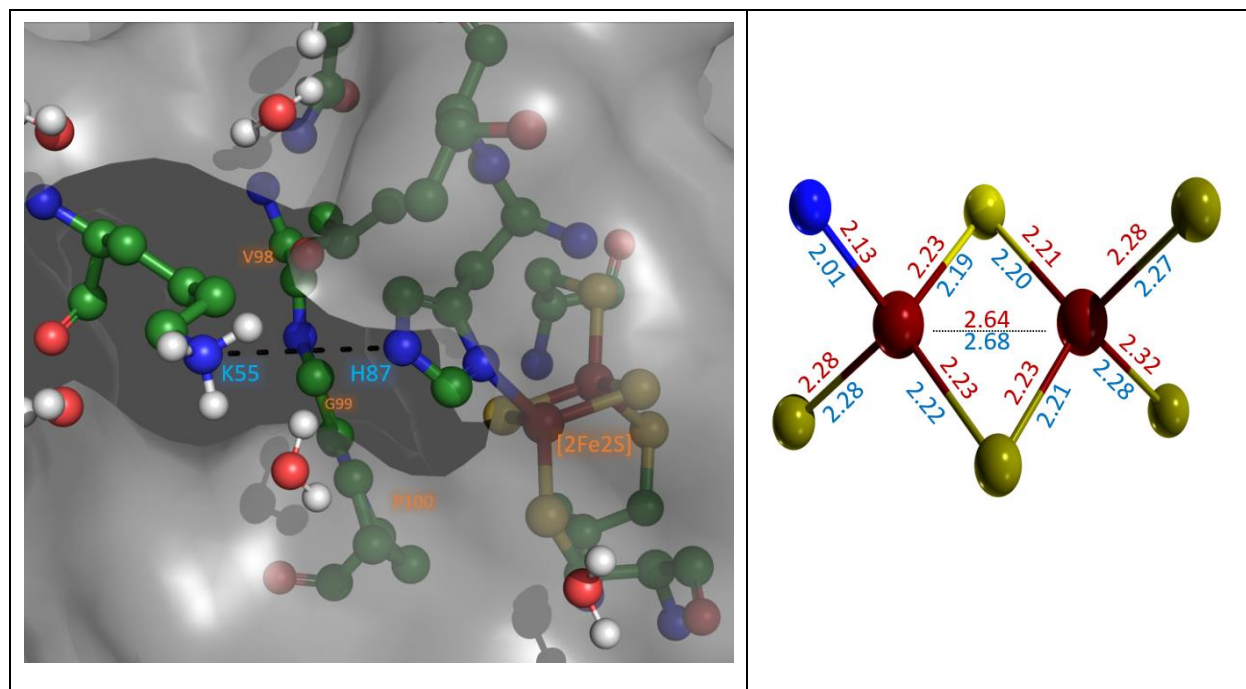


Figure 4. Left: His-87 and Lys-55 with the protein cleft (Val-98, Gly-99, Pro-100), grey represents the Connolly³⁶ (solvent access) surface excluding His-87 and Lys-55, the dashed black line connects the two heavy (nitrogen) atoms within hydrogen bonding distance as found in PDB 2QH7.¹³ **Right:** The core atoms of the geometry optimized structure of the mNT [2Fe-2S] cluster. Labels indicate bond lengths in Angstroms for the oxidized imidazolate-bound (blue) and reduced imidazole-bound (red) clusters.

Summary

Here we have demonstrated the utility of ⁵⁷Fe NRVS to probe the Fe-His interaction in both reduced and oxidized mNT [2Fe-2S] cluster. Unlike resonance Raman spectroscopy, NRVS does not depend on optical excitations and thus we were able to characterize the reduced Fe-N_s bond for the first time - it does not have excitation bands amenable to resonance Raman²³, and there are no crystal structures available for the mNT in the reduced state. The Fe-N bond is stronger in the oxidized form, however the protein is more susceptible to cluster loss in this form.¹⁹ We identify the dynamic solvation of the protein

cleft proximal to the cluster-coordinating histidine as a potential factor facilitating cluster loss consistent with previous molecular dynamics studies.²⁵ This work highlights the strengths of ⁵⁷Fe NRVs to obtain detailed geometric and vibrational insights into Fe-S clusters that are not accessible through conventional methods.

ASSOCIATED CONTENT

Accession Code

UniProt: mitoNEET – CSD1: Q9NZ45

Supporting Information

The Supporting Information is available free of charge at

<https://pubs.acs.org/doi/10.1021/acs.biochem...>

Experimental and computational procedures and supplementary Figures S1–S4 and Table S1 (PDF)

Animations (GIF format) showing the DFT-calculated normal modes (ZIP)

Cartesian (XYZ format) coordinates of the DFT-optimized structures (ZIP)

AUTHOR INFORMATION

- Corresponding Authors

Stephen P. Cramer – *SETI Institute, Mountain View, CA 94043 USA*

- Authors

Leland B. Gee – LCLS, SLAC National Accelerator Laboratory, Menlo Park, California 94025, USA

Vladimir Pelmenschikov – *Institut für Chemie, Technische Universität Berlin, 10623 Germany*

Cécile Mons – *Institut de Chimie des Substances Naturelles (ICSN), CNRS UPR 2301, Université Paris-Saclay, 91198 Gif-sur-Yvette cedex, France*

Nakul Mishra – *Department of Chemistry, University of California, Davis, CA, 95616, USA*

Hongxin Wang – *SETI Institute, Mountain View, CA 94043, USA*

Yoshitaka Yoda – *Precision Spectroscopy Division, SPring-8/JASRI, 1-1-1 Kouto, Sayo, Hyogo 679-5198, JAPAN*

Kenji Tamasaku – *Materials Dynamics Laboratory, RIKEN SPring-8, 1-1-1 Kouto, Sayo, Hyogo 679-5148, JAPAN*

Marie-Pierre Golinelli-Cohen – *Institut de Chimie des Substances Naturelles (ICSN), CNRS UPR 2301, Université Paris-Saclay, 91198 Gif-sur-Yvette cedex, France*

Acknowledgments

The work by V.P. was funded by the Deutsche Forschungsgemeinschaft (DFG, German Research Foundation) under Germany's Excellence Strategy – EXC 2008 – 390540038 – UniSysCat. M.-P.G.-C. warmly acknowledges the networking support from the EU COST Action FeSBioNet (CA15133). S.P.C. was funded by NIH GM65440. Some computational work was performed under the XSIM project on the CORI computing system at NERSC a U.S. Department of Energy Office of Science User Facility operated under Contract No. DE-AC02-05CH11231.

References

1. Tamir, S.; Paddock, M. L.; Darash-Yahana-Baram, M.; Holt, S. H.; Sohn, Y. S.; Agranat, L.; Michaeli, D.; Stofleth, J. T.; Lipper, C. H.; Morcos, F.; Cabantchik, I. Z.; Onuchic, J. N.; Jennings, P. A.; Mittler, R.; Nechushtai, R., Structure-function analysis of NEET proteins uncovers their role as key regulators of iron and ROS homeostasis in health and disease. *Biochimica Et Biophysica Acta-Molecular Cell Research* **2015**, *1853* (6), 1294-1315.
2. Colca, J. R.; McDonald, W. G.; Waldon, D. J.; Leone, J. W.; Lull, J. M.; Bannow, C. A.; Lund, E. T.; Mathews, W. R., Identification of a novel mitochondrial protein ("mitoNEET") cross-linked specifically by a thiazolidinedione photoprobe. *Am. J. Physiol.-Endocrinol. Metab.* **2004**, *286* (2), E252-E260.
3. Moreno-Navarrete, J. M.; Moreno, M.; Ortega, F.; Sabater, M.; Xifra, G.; Ricart, W.; Fernandez-Real, J. M., CISD1 in association with obesity-associated dysfunctional adipogenesis in human visceral adipose tissue. *Obesity (Silver Spring)* **2016**, *24* (1), 139-47.
4. Kusminski, C. M.; Holland, W. L.; Sun, K.; Park, J.; Spurgin, S. B.; Lin, Y.; Askew, G. R.; Simcox, J. A.; McClain, D. A.; Li, C.; Scherer, P. E., MitoNEET-driven alterations in adipocyte mitochondrial activity reveal a crucial adaptive process that preserves insulin sensitivity in obesity. *Nature Medicine* **2012**, *18* (10), 1539-U144.
5. Ferecatu, I.; Gonçalves, S.; Golinelli-Cohen, M.-P.; Clémancey, M.; Martelli, A.; Riquier, S.; Guittet, E.; Latour, J.-M.; Puccio, H.; Drapier, J.-C.; Lescop, E.; Bouton, C., The Diabetes Drug Target MitoNEET Governs a Novel Trafficking Pathway to Rebuild an Fe-S Cluster into Cytosolic Aconitase/Iron Regulatory Protein 1. *J. Biol. Chem.* **2014**, *289* (41), 28070-28086.
6. Chen, X. Y.; Ren, H. H.; Wang, D.; Chen, Y.; Qu, C. J.; Pan, Z. H.; Liu, X. N.; Hao, W. J.; Xu, W. J.; Wang, K. J.; Li, D. F.; Zheng, Q. S., Isoliquiritigenin Induces Mitochondrial Dysfunction and Apoptosis by Inhibiting mitoNEET in a Reactive Oxygen Species-Dependent Manner in A375 Human Melanoma Cells. *Oxid Med Cell Longev* **2019**, *2019*, 9817576.
7. Sohn, Y. S.; Tamir, S.; Song, L. H.; Michaeli, D.; Matouk, I.; Conlan, A. R.; Harir, Y.; Holt, S. H.; Shulaev, V.; Paddock, M. L.; Hochberg, A.; Cabanchick, I. Z.; Onuchic, J. N.; Jennings, P. A.; Nechushtai, R.; Mittler, R., NAF-1 and mitoNEET are central to human breast cancer proliferation by maintaining mitochondrial homeostasis and promoting tumor growth. *Proc. Natl. Acad. Sci. U. S. A.* **2013**, *110* (36), 14676-14681.
8. Karmi, O.; Marjault, H. B.; Pesce, L.; Carloni, P.; Onuchic, J. N.; Jennings, P. A.; Mittler, R.; Nechushtai, R., The unique fold and lability of the 2Fe-2S clusters of NEET proteins mediate their key functions in health and disease. *J. Biol. Inorg. Chem.* **2018**, *23* (4), 599-612.
9. Mittler, R.; Darash-Yahana, M.; Sohn, Y. S.; Bai, F.; Song, L. H.; Cabantchik, I. Z.; Jennings, P. A.; Onuchic, J. N.; Nechushtai, R., NEET Proteins: A New Link Between Iron Metabolism, Reactive Oxygen Species, and Cancer. *Antioxidants & Redox Signaling* **2019**, *30* (8), 1083-1095.
10. Geldenhuys, W. J.; Benkovic, S. A.; Lin, L.; Yonutas, H. M.; Crish, S. D.; Sullivan, P. G.; Darvesh, A. S.; Brown, C. M.; Richardson, J. R., MitoNEET (CISD1) Knockout Mice Show Signs of Striatal Mitochondrial Dysfunction and a Parkinson's Disease Phenotype. *Acs Chemical Neuroscience* **2017**, *8* (12), 2759-2765.
11. Zuris, J. A.; Harir, Y.; Conlan, A. R.; Shvartsman, M.; Michaeli, D.; Tamir, S.; Paddock, M. L.; Onuchic, J. N.; Mittler, R.; Cabantchik, Z. I.; Jennings, P. A.; Nechushtai, R., Facile transfer of 2Fe-2S clusters from the diabetes drug target mitoNEET to an apo-acceptor protein. *Proc. Natl. Acad. Sci. U. S. A.* **2011**, *108* (32), 13047-13052.

12. Mons, C.; Botzanowski, T.; Nikolaev, A.; Hellwig, P.; Cianferani, S.; Lescop, E.; Bouton, C.; Golinelli-Cohen, M. P., The H₂O₂-Resistant Fe-S Redox Switch MitoNEET Acts as a pH Sensor to Repair Stress-Damaged Fe-S Protein. *Biochemistry* **2018**, *57* (38), 5616-5628.
13. Paddock, M. L.; Wiley, S. E.; Axelrod, H. L.; Cohen, A. E.; Roy, M.; Abresch, E. C.; Capraro, D.; Murphy, A. N.; Nechushtai, R.; Dixon, J. E.; Jennings, P. A., MitoNEET is a uniquely folded 2Fe-2S outer mitochondrial membrane protein stabilized by pioglitazone. *Proc. Natl. Acad. Sci. U. S. A.* **2007**, *104* (36), 14342-14347.
14. Hou, X. W.; Liu, R. J.; Ross, S.; Smart, E. J.; Zhu, H. N.; Gong, W. M., Crystallographic studies of human MitoNEET. *J. Biol. Chem.* **2007**, *282* (46), 33242-33246.
15. Lin, J. Z.; Zhou, T.; Ye, K. Q.; Wang, J. F., Crystal structure of human mitoNEET reveals distinct groups of iron-sulfur proteins. *Proc. Natl. Acad. Sci. U. S. A.* **2007**, *104* (37), 14640-14645.
16. Bak, D. W.; Zuris, J. A.; Paddock, M. L.; Jennings, P. A.; Elliott, S. J., Redox characterization of the FeS protein MitoNEET and impact of thiazolidinedione drug binding. *Biochemistry* **2009**, *48* (43), 10193-5.
17. Bak, D. W.; Elliott, S. J., Alternative FeS cluster ligands: tuning redox potentials and chemistry. *Current Opinion in Chemical Biology* **2014**, *19*, 50-58.
18. Bergner, M.; Dechert, S.; Demeshko, S.; Kupper, C.; Mayer, J. M.; Meyer, F., Model of the MitoNEET [2Fe-2S] Cluster Shows Proton Coupled Electron Transfer. *J Am Chem Soc* **2017**, *139* (2), 701-707.
19. Golinelli-Cohen, M. P.; Lescop, E.; Mons, C.; Goncalves, S.; Clemancey, M.; Santolini, J.; Guittet, E.; Blondin, G.; Latour, J. M.; Bouton, C., Redox Control of the Human Iron-Sulfur Repair Protein MitoNEET Activity via Its Iron-Sulfur Cluster. *The Journal of biological chemistry* **2016**, *291* (14), 7583-93.
20. Wiley, S. E.; Paddock, M. L.; Abresch, E. C.; Gross, L.; van der Geer, P.; Nechushtai, R.; Murphy, A. N.; Jennings, P. A.; Dixon, J. E., The outer mitochondrial membrane protein mitoNEET contains a novel redox-active 2Fe-2S cluster. *The Journal of biological chemistry* **2007**, *282* (33), 23745-9.
21. Dicus, M. M.; Conlan, A.; Nechushtai, R.; Jennings, P. A.; Paddock, M. L.; Britt, R. D.; Stoll, S., Binding of histidine in the (Cys)₃(His)₁-coordinated [2Fe-2S] cluster of human mitoNEET. *J Am Chem Soc* **2010**, *132* (6), 2037-49.
22. Iwasaki, T.; Samoilova, R. I.; Kounosu, A.; Ohmori, D.; Dikanov, S. A., Continuous-wave and pulsed EPR characterization of the [2Fe-2S](Cys)₃(His)₁ cluster in rat MitoNEET. *J Am Chem Soc* **2009**, *131* (38), 13659-67.
23. Tirrell, T. F.; Paddock, M. L.; Conlan, A. R.; Smoll, E. J.; Nechushtai, R.; Jennings, P. A.; Kim, J. E., Resonance Raman Studies of the (His)(Cys)₃ 2Fe-2S Cluster of MitoNEET: Comparison to the (Cys)₄ Mutant and Implications of the Effects of pH on the Labile Metal Center. *Biochemistry* **2009**, *48* (22), 4747-4752.
24. Baxter, E. L.; Zuris, J. A.; Wang, C.; Vo, P. L. T.; Axelrod, H. L.; Cohen, A. E.; Paddock, M. L.; Nechushtai, R.; Onuchic, J. N.; Jennings, P. A., Allosteric control in a metalloprotein dramatically alters function. *Proc. Natl. Acad. Sci. U. S. A.* **2013**, *110* (3), 948-953.
25. Pesce, L.; Calandrini, V.; Majault, H. B.; Lipper, C. H.; Rossetti, G.; Mittler, R.; Jennings, P. A.; Bauer, A.; Nechushtai, R.; Carloni, P., Molecular Dynamics Simulations of the 2Fe-2S Cluster-Binding Domain of NEET Proteins Reveal Key Molecular Determinants That Induce Their Cluster Transfer/Release. *Journal of Physical Chemistry B* **2017**, *121* (47), 10648-10656.

26. Xiao, Y.; Tan, M.-L.; Ichiye, T.; Wang, H.; Guo, Y.; Smith, M. C.; Meyer, J.; Sturhahn, W.; Alp, E. E.; Zhao, J.; Yoda, Y.; Cramer, S. P., Dynamics of *Rhodobacter capsulatus* [2Fe-2S] Ferredoxin VI and *Aquifex aeolicus* Ferredoxin 5 via Nuclear Resonance Vibrational Spectroscopy (NRVS) and Resonance Raman Spectroscopy. *Biochemistry* **2008**, *47* (25), 6612–6627.
27. Lauterbach, L.; Gee, L. B.; Pelmeshnikov, V.; Jenney, F. E.; Kamali, S.; Yoda, Y.; Adams, M. W.; Cramer, S. P., Characterization of the [3Fe-4S](0/1+) cluster from the D14C variant of *Pyrococcus furiosus* ferredoxin via combined NRVS and DFT analyses. *Dalton Trans* **2016**, *45* (17), 7215-9.
28. Han, S.; Czernuszewicz, R. S.; Kimura, T.; Adams, M. W. W.; Spiro, T. G., Fe₂S₂ Protein Resonance Raman Revisited: Structural Variations among Adrenodoxin, Ferredoxin, and Red Paramagnetic Protein. *Journal of the American Chemical Society* **1989**, *111* (10), 3505-3511.
29. Rotsaert, F. A. J.; Pikus, J. D.; Fox, B. G.; Markley, J. L.; Sanders-Loehr, J., N-isotope effects on the Raman spectra of Fe₂S₂ ferredoxin and Rieske ferredoxin: evidence for structural rigidity of metal sites. *J. Biol. Inorg. Chem.* **2003**, *8* (3), 318-326.
30. Kuila, D.; Schoonover, J. R.; Dyer, R. B.; Batie, C. J.; Ballou, D. P.; Fee, J. A.; Woodruff, W. H., Resonance Raman Studies of Rieske-Type Proteins. *Biochim. Biophys. Acta* **1992**, *1140* (2), 175-183.
31. Schott, J.; Dreybrodt, W.; Schweitzer-Stenner, R., The Fe²⁺-His(F8) Raman band shape of deoxymyoglobin reveals taxonomic conformational substates of the proximal linkage. *Biophysical Journal* **2001**, *81* (3), 1624-1631.
32. Gilch, H.; Schweitzerstenner, R.; Dreybrodt, W., Structural Heterogeneity of the Fe²⁺-N-Epsilon(His(F8)) Bond in Various Hemoglobin And Myoglobin Derivatives Probed by the Raman-Active Iron Histidine Stretching Mode. *Biophysical Journal* **1993**, *65* (4), 1470-1485.
33. Gurbiel, R. J.; Batie, C. J.; Sivaraja, M.; True, A. E.; Fee, J. A.; Hoffman, B. M.; Ballou, D. P., Electron-nuclear double resonance spectroscopy of nitrogen-15-enriched phthalate dioxygenase from *Pseudomonas cepacia* proves that two histidines are coordinated to the [2Fe-2S] Rieske-type clusters. *Biochemistry* **1989**, *28* (11), 4861-4871.
34. Tang, Q.; Kalsbeck, W. A.; Olson, J. S.; Bocian, D. F., Disruption of the Heme Iron-Proximal Histidine Bond Requires Unfolding of Deoxymyoglobin. *Biochemistry* **1998**, *37* (19), 7047-7056.
35. Bak, D. W.; Elliott, S. J., Conserved Hydrogen Bonding Networks of MitoNEET Tune Fe-S Cluster Binding and Structural Stability. *Biochemistry* **2013**, *52* (27), 4687-4696.
36. Connolly, M. L., Analytical molecular surface calculation. *Journal of Applied Crystallography* **1983**, *16* (5), 548-558.